3D-printed structured catalysts for CO_2 methanation reaction: Advancing of gyroid-based geometries

Miriam González-Castaño [a,*], Francisco Baena-Moreno [a,b,c], Juan Carlos Navarro de Miguel [d], Kamal U.M. Miah [e], Fátima Arroyo-Torralvo [b], Ralf Ossenbrink [e], Jose Antonio Odriozola [d,f], Walther Benzinger [g], Andreas Hensel [g], Achim Wenka [g], Harvey Arellano-García [a,f]

[a] Department of Process and Plant Technology, Brandenburg University of Technology (BTU) Cottbus-Senftenberg, 03046 Cottbus, Germany
[b] Chemical and Environmental Engineering Department, Technical School of Engineering, University of Seville, 41092 Seville, Spain
[c] Department of Space, Earth, and Environment, Chalmers University of Technology, 412 96 Goteborg, Sweden
[d] Department of Inorganic Chemistry and Materials Science Institute of Seville Mixed Centre University of Seville, CSIC, 41092 Seville, Spain
[e] Department of Joining and Welding Technology, Brandenburg University of Technology (BTU) Cottbus-Senftenberg, 03046 Cottbus, Germany
[f] Department of Chemical and Process Engineering, University of Surrey, Guildford Surrey GU2 7XH, United Kingdom
[g] Institute for Micro Process Engineering (IMVT), Karlsruhe Institue of Technology (KIT), 76021 Karlsruhe, Germany

ARTICLE INFO

Keywords:
3D-printing
Triply periodic minimal surfaces
Fluid guiding elements
CO_2 methanation
Structured catalysts
Experiment design

ABSTRACT

This work investigates the CO_2 methanation rate of structured catalysts by tuning the geometry of 3D-printed metal Fluid Guiding Elements (FGEs) structures based on periodically variable pseudo-gyroid geometries. The enhanced performance showed by the structured catalytic systems is mostly associated with the capability of the FGEs substrate geometries for efficient heat usages. Thus, variations on the channels diameter resulted in ca. 25% greater CO_2 conversions values at intermediate temperature ranges. The highest void fraction evidenced in the best performing catalyst (3D-1) favored the radial heat transfer and resulted in significantly enhanced catalytic activity, achieving close to equilibrium (75%) conversions at 400 °C and 120 mL/min. For the 3D-1 catalyst, a mathematical model based on an experimental design was developed thus enabling the estimation of its behavior as a function of temperature, spatial velocity, hydrogen to carbon dioxide (H_2/CO_2) ratio, and inlet CO_2 concentration. Its optimal operating conditions were established under 3 different scenarios: 1) no restrictions, 2) minimum H_2:CO_2 ratios, and 3) minimum temperatures and H_2/CO_2 ratio. For instance, for the lattest scenario, the best CO_2 methanation conditions require operating at 431 °C, 200 mL/min, $H_2/CO_2 = 3$ M ratio, and inlet CO_2 concentration = 10 %.

1. Introduction

The production of synthetic natural gas (SNG) through the hydrogenation of CO_2 feedstock using renewable H_2 as a source is regarded as an appealing route towards the production of biofuels and therefore, towards the implementation of sustainable circular energy models [1]. Nevertheless, the use of CO_2 as a building block for the generation of methane via the CO_2 methanation reaction ($CO_2 + 4H_2 \quad CH_4 + H_2O$) requires the development of highly active and efficient catalytic systems capable of yielding CH_4 in a selective manner [2]. For that purpose, employing adequate catalytic formulations becomes mandatory with Ni-based options often proposed as suitable systems since they couple optimal hydrogenation rates with fair prices [3–5].

Furthermore, fine thermal management constitutes an essential aspect to consider for maximizing the efficiency of the CO_2 hydrogenation unit [6]. Certainly, the control of the temperature is one of the major issues during the CO_2 methanation reaction [7]. In this sense, the use of structured catalysts, where the catalyst active phase is coated over metallic substrates, enhances the thermal control of the catalytic reactor and enables exploiting the maximum capacity of a given catalytic system

Abbreviations: FGEs, fluid guiding elements; PC-HC, parallel channel honeycomb; SV, space velocity; $N_{External\ Channels}$, number of external channels constituting the metal substrate; $N_{Internal\ Channels}$, number of internal channels constituting the metal substrate; Angle G, orientation angle of gyroid; V_{SP}, volume of the spacer; A_{inner}, inner area; V_T, total volume; ε, porosity; Dh, hydraulic diameter; df, degree of freedom; F-value, value of Fisheŕs ratio; p-value, probability value.

* Corresponding author.
E-mail address: gonzalez@b-tu.de (M. González-Castaño).

[6,8,9].

The benefits of employing structured catalysts in thermocatalytic processes have been extensively reviewed elsewhere [10,11]. In short, the miniaturization of the distances established within the microchannel (or micro-sized geometries) conforming the metal substrates promotes the diffusional processes and enables better control of the reaction temperature throughout the catalyst bed. Compared with fixed-bed reactor configurations, the thermal distribution improvement achieved by employing metal substrates minimizes the hot spots constitution and constricts the problematic sintering phenomena typically described as Ni catalysts [12,13]. Additionally, considering that the competitive Reverse Water Gas Shift (R-WGS) reaction plays an important role at temperatures above 450 °C [14], optimal temperature management also facilitates maintaining high selectivity towards CH_4 and enhances the overall catalyst performance.

The benefits attained in structured catalysts and the influence of the metal substrate geometry on the CO_2 methanation performance for Ni-Ru/Mg-Al catalysts were recently demonstrated [15,16]. The improved catalytic performance displayed by metal substrates based on pseudo-gyroid geometries compared to the traditional honeycomb monoliths was associated with the enhanced mass and heat transport phenomena. Thus, with respect to the characteristic laminar flows and, in consequence, poor mixing achieved within the parallel channels of honeycomb metal substrates, the enhanced performance of the gyroid-based structured catalyst were associated with increased heat transfer due to improved flow. Similarly, the benefits of adequate thermal management on the CO_2 methanation performance of structured catalysts have been claimed [17,18]. García-Moncada et al. [18] associated the improved CO_2 methanation rates exhibited by Ni/CeO_2 structured catalysts with more homogeneous thermal profiles and better catalysts usage.

Despite the increasing interest in the CO_2 methanation reaction, development of novel strategies for improving the thermal management of the catalytic systems through utilization of structured catalysts is somewhat limited. In fact, the scarcity of studies using honeycomb and sponges metal substrates for structured catalysts becomes significantly more notable when it comes to the employment of complex geometries [19].

The potential of 3D printing technologies for designing catalytic systems [20,21] with advanced thermal profiles by the application of Fluid Guiding Elements (FGEs) as metal substrates was recently claimed by Hansjosten et al [22]. It is proposed that more efficient uses of the energy employed for heating the catalytic reactor could be attained by guiding the gas mixture through an optimal flowing pattern. Considering that the heat transfer of a gas mixture heated by a hot wall is determined by the thermal gradient established within the boundary layer of the fluid, maximizing the gradient throughout the catalyst bed must benefit the thermal profile of the catalyst. In this sense, FGEs facilitate the subdivision of the total flow in several partial flows which are guided towards and away from the heating wall in such a way that a large temperature gradient is maintained.

In this context, this work aims at boosting the catalytic activity of structured catalysts for the CO_2 methanation reaction by tuning the geometry of the FGEs as metal substrates. To the best of our knowledge, assessing the impact of the geometric variations of gyroid based metal substrates on the CO_2 methanation catalytic performance has never been attempted.

For this purpose, a series of FGEs metal substrates based on gyroid geometries with different unit cell dimensions were manufactured by selective laser melting and subsequently, washcoated with 0.5% Ru 15% $Ni/MgAl_2O_4$ catalyst [23]. Fig. 1 illustrates the geometric variations attained on the metal substrates. Thus, different numbers and sizes of the constituting channels were obtained as a function of the polar radius of the gyroid, the orientation angle of gyroids which is creating the volume of the spacer Therefore, the catalytic activity exhibited by the manufactured structured catalysts as a function of the geometry was evaluated and rationalized for the CO_2 methanation reaction.

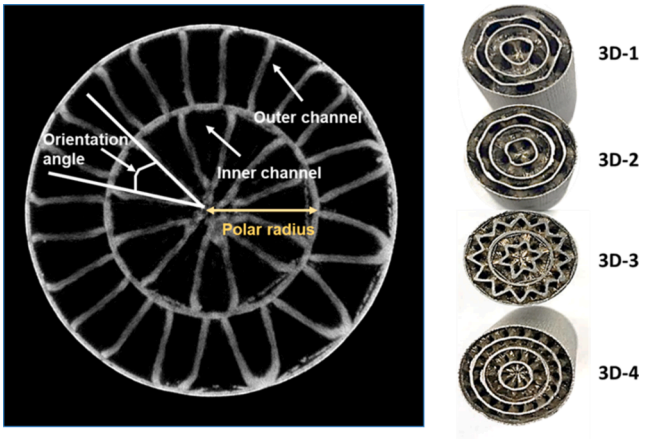

Fig. 1. 3D-printed FGEs substrates.

Subsequently, the structured catalyst with the best performance in terms of the methanation efficiency is subjected to an experimental design in order to obtain a model of the system for the selected parameters: temperature, spatial velocity, hydrogen to carbon dioxide (H_2/CO_2) ratio, and inlet CO_2 concentration. This model can predict the CO_2 conversion within the range of values tested, quantifying the influence of the variables said. For the latter aim, the experimental design was elaborated with the software DesignExpert v9.0.6.

2. Materials and methods

2.1. Fluid guiding elements (FGEs)

The geometry of the manufactured stainless-steel metal substrates was inspired by a patent [24] to control reactions and processes by improving heat and mass transfer. 3D printing gives the possibility of manufacturing very special geometrical designs with properties that cannot be produced conventionally. These geometrical internal designs influence the performance of heat exchangers or chemical rectors significantly in terms of efficiency or product quality. The structure and thus the performance of such structures are a function of the geometry. Thus, 3D printing of metallic structures as tube inserts mainly influence the fluid flow by guiding the flow along given paths. In Fig. 2 a fluid guiding unit (FGU), which is the base of a FGEs (several units form at least one element) is shown.

The basis of the bended surfaces are so called freeform surfaces (B-

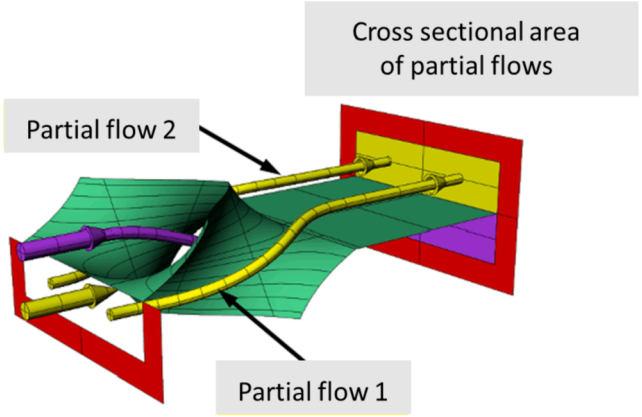

Fig. 2. Sketch of the fluid guiding unit (FGU) with the flow path along the bended surfaces showing the subdivision of the flow and the exchange of the positions of the partial flows.

splines). The target is not to attain turbulent flow conditions, but to guide the flow along the flow paths. Guiding the flow along the different flow paths results in an alternatingly contact with the heat transferring wall of the tube, with the consequence of a high heat transfer coefficient locally. This can be due to the constantly changing cross-section, which in consequence causes also changing velocities of the flow. This in turn affects the heat transfer coefficient α. Since catalytic reactions are linked to a generation of heat, it can be assumed that the improved heat transfer is also beneficial for the catalytic reactions. Changing flow rates will also influence adsorption/desorption processes of the catalytic reactions. Thus, changing velocities of the flow and an increased heat transfer coefficient, make the FGEs candidates for use in catalytic reactions [22].

The modular character of the FGU enables a connection in series or in parallel. If the FGU are arranged one above the other, a completely different flow pattern results (Fig. 3). The flow is subdivided in three partial flows exchanging their position along the flow direction. The flow returns to the starting position through three FGUs in the flow direction. In Fig. 4 the FGU parallelized one next to the other does not change the flow pattern.

The construction of the FGEs offers the possibility to obtain a tailored FGEs for the respective process by combining various parameters such as channel width, channel length, or number of partial flows. Therefore, for a given process the reaction conditions can be adjusted by a combination of a set of geometric parameters. In order to explain the working principle of the FGE, the basic elements, the FGUs, are shown in a planar arrangement for a better overview (Figs. 2-4). The planar arrangement of the FGU can be arranged in a circle around an axis, resulting in a modular system that is very easy to insert into tubes and tube gaps (Fig. 5).

2.2. Materials

- *3D printing of metal substrates*

Fig. 6 depicts the CT-XRD (Computed Tomography X-Ray Diffraction) images obtained for the different printed micromonoliths where, as it can be observed, the *size* of the filling pseudo-gyroid motive decreases sequentially according to the following trend: 3D-1 > 3D-2 > 3D-3 > 3D-4. Thus, the 3D-CAD model was used for generating the outer cylinder whilst the inside of the cylinder was filled with the circular FGU in a form of a pseudo-gyroid structure. The monoliths were manufactured employing an SLM-125 3D metal printer from Realizer GmbH. The SLM-125 was equipped with a 400 W laser. Before the washcoating process, all metal substrates were annealed in air at 900 °C for 12 h.

- *Catalyst synthesis and the washcoating process*

The $MgAl_2O_4$ support was prepared by impregnating an ethanolic solution of $Mg(NO_3)_2{\cdot}6H_2O$ (Aldrich) over commercial alumina powder in order to achieve 10 wt% MgO. The impregnated solid was dried overnight and calcined at 850 °C during 12 h. Afterward, co-impregnation of 15 wt% Ni and 0.5 wt% Ru using their corresponding

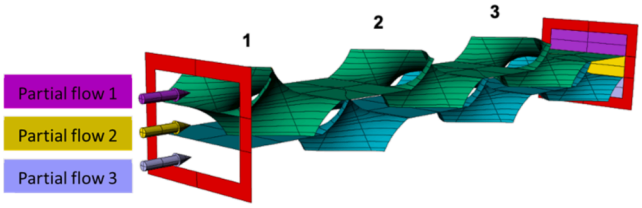

Fig. 3. Parallelized Fluid guiding unit (FGU) one above the other resulting in a new flow pattern. After three FGUs in the flow direction the original position recurs.

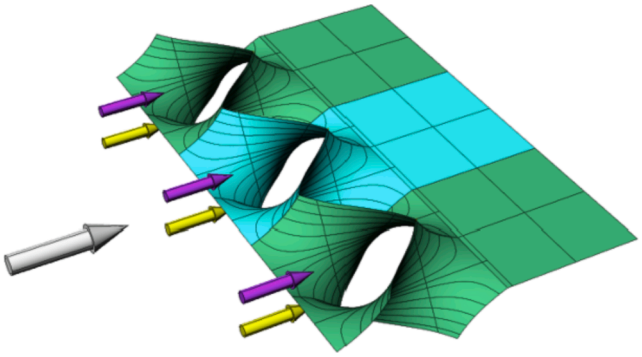

Fig. 4. Parallelized Fluid guiding unit (FGU) resulting in an unchanged guiding of the flow by the bended surfaces.

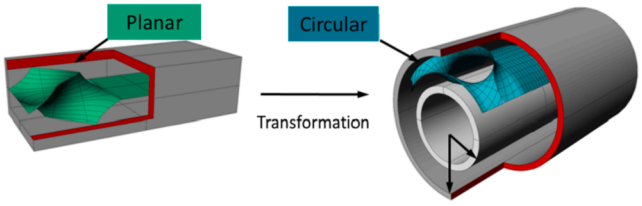

Fig. 5. Transformation of the planar geometry to a circular shaped geometry for use in tubes.

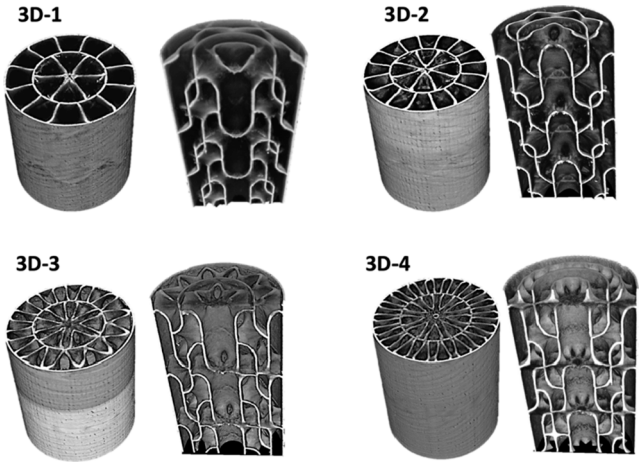

Fig. 6. CT-XRD of the prepared 3D-printed FGEs metal substrates.

nitrates precursors ($Ni(NO_3)_2{\cdot}6H_2O$ and $Ru(NO)(NO_3)_3$, Aldrich) was conducted. The obtained solids were dried and calcined at 500 °C during 5 h [15].

The obtained catalyst was grinded in a zirconia mill ball and the suspension employed for the washcoating procedure was prepared using the catalyst fraction with particle sizes around 10 μm. The washcoating suspension contained 18.2 wt% catalyst, 74.62 wt% deionized water, 6.06 wt% colloidal alumina (Nyacol Al20), and 1.14 wt% poly(vinyl alcohol) (PVA). The pH was fixed to 7.1 using diluted NH_3 solution.

Thus, once the slurry was prepared, the metal substrates were immersed in the stirred slurry at 2 cm/s and the excess was blown out, resulting in *ca.* 50–60 mg of catalyst coated per cycle. The coated metal substrates were calcined at 500 °C during 4 h. All samples were washcoated with 0.220 (±0.017) g of catalyst.

2.3. Methods

- *Catalytic activity and thermographs*

The catalytic activity of the structured catalysts was measured in a tubular reactor (internal diameter 17 mm). The structured catalysts were pre-reduced employing 10% H_2:N_2 streams at 600 °C during 2 h. The catalyst performance was evaluated in the 150–400 °C temperature range at 120 L/gh (400 mL/min – 0.2 g_{cat}) and under feed streams composed of 15% CO_2 + 60% H_2 + 25% N_2. The inlet and outlet compositions were analysed with an ABB analyser suited with IR and TCD detectors. Reproducibility checks were conducted resulting in an overall experimental error of ± 3%. The CO_2 conversion and CH_4/CO selectivity were calculated according to Equations (1), 2 and 3, respectively.

$$CO_2\text{conversion}(\%) \quad \frac{[F_{CO2in} \quad F_{CO2out}]}{F_{CO2in}} x100 \tag{1}$$

$$CH_4\text{selectivity}(\%) \quad \frac{[CH_{4out}]}{[CO_{2in}] \quad [CO_{2out}]} x100 \tag{2}$$

$$CO\text{selectivity}(\%) \quad \frac{[CO_{out}]}{[CO_{2in}] \quad [CO_{2out}]} x100 \tag{3}$$

The thermographs were obtained by recording the temperature profile exhibited by the samples in contact with a hot plate at 300 °C on a VarioCam ® HDx 645 using a 1280 × 960 Resolution (Pixel size) and a 30 Hz frame rate.

- *Experimental Design*

Table 1 shows the values for the four parameters of each experiment designed with the software DesignExpert v9.0.6. After performing the experiments, the results obtained were fitted using a polynomial model (Equation (4)). In Equation (4), X are the parameters (temperature, space velocity, H_2/CO_2 molar ratio, inlet CO_2 concentration) values, β are the modelled coefficients, and Y is the response (CO_2 conversion).

Table 1
Experimental design matrix for the first round of experiments.

Test	T (°C)	SV (mL/min)	H_2/CO_2 ratio (mol/mol)	CO_2 concentration (%)
1	500	400	4	20
2	350	300	3	5
3	200	400	2	20
4	500	400	2	10
5	350	300	3	15
6	350	300	3	25
7	500	200	4	10
8	200	400	4	10
9	350	300	3	15
10	650	300	3	15
11	350	500	3	15
12	500	200	2	20
13	350	300	3	15
14	350	300	5	15
15	200	400	4	20
16	350	300	3	15
17	200	400	2	10
18	350	300	1	15
29	500	200	4	20
20	500	400	2	20
21	500	200	2	10
22	350	300	3	15
23	500	400	4	10
24	200	200	4	10
25	200	200	2	10
26	350	100	3	15
27	200	200	4	20
28	200	200	2	20
29	350	300	3	15

The statistical significance was evaluated using the F-test. The space of interest for the parameters analyzed has the following ranges: temperature 200–500 °C; Space Velocity (SV) 100–400 mL/min; H_2/CO_2 molar ratio 4 ; and inlet CO_2 concentration 5–20%, where confidence levels are considered.

$$Y \quad \beta_0 + \sum_{i\ 1}^{4} \beta_i X_i + \sum_{i\ 1}^{4} \beta_{ii} X_{ii}^2 + \sum_{i\ 1}^{3} \sum_{j\ 2}^{4} \beta_{ij} X_i X_j \tag{4}$$

3. Results

SEM images of the structured catalysts (Figure S1) showed comparable catalyst layer morphologies and compositions, in agreement with previous works. Table 2 shows the geometrical features of the the 3D-printed FGEs metal substrates. In agreement with Figs. 1 and 2, the number of channels of the structured systems increases according to the sequence: 3D-1 < 3D-2 < 3D-3 < 3D-4. As expected, the porosity (ε, Equation (5)) of the FGEs metal substrates also decreased as the number of channels increased.

$$\varepsilon \quad 1 \quad \frac{V_{SP}}{V_T} \tag{5}$$

Fig. 7 presents the catalytic activity exhibited by the catalyst series at 120 L/gh and H_2/CO_2 ratios of 4. For all catalytic systems, the CO_2 conversion increased with the reaction temperature depicting the sinusoidal profile characteristic of exothermal reactions kinetically limited within the lower temperature range, but thermodynamically limited at higher temperature windows [25]. Thus, the catalytic activity of the samples decreased according to the sequence: 3D-1 > 3D-4 ~ 3D-3 > 3D-2 with the 3D-1 catalyst (the catalyst supported over the metal substrate with the highest channels diameter) exhibiting the best conversion rates.

Nonetheless, it is worth mentioning that a linear relationship between the number of channels (or channels diameter) and the performance was not observed for the catalyst series investigated here. Moreover, all 3D-printed structured catalysts displayed better performance compared to the PC-HC (parallel channel honeycomb) monolith, used as a reference in this work. Furthermore, in terms of the CH_4 selectivity, for which significant yields were achieved by all systems, all 3D-metal substrates outperformed the PC-HC micromonolith.

The catalytic improvement obtained for the different metal substrates should be uniquely ascribed to the different geometries exhibited by the FGEs. Considering the geometry of the catalytic system, where the heat is supplied to the catalysts through an external wall, the catalytic activity of the structured catalysts should be determined by the amount of heat effectively transferred from the wall, i.e., the radial heat transfer of the systems. Assuming that the heat supplied by the furnace is constant for all the evaluated samples, the conversion attained by the catalysts should be proportional to the energy effectively used for the reaction. In other words, the attained conversion values underline the ability of the different metal substrates for transfering heat towards the longitudinal axis of the structured catalysts. Thus, the better the

Table 2
Geometrical features of the 3D-printed FGEs metal substrates.

	Geometry				
	PC-HC	3D- 1	3D-2	3D-3	3D-4
$N_{External\ Channels}$	–	12	16	24	36
$N_{Internal\ Channels}$	–	6	8	12	18
Angle G (°)	–	60	45	20	30
V_{SP} (mm^3)	–	4220	4359	4310	3826
V_{SP}/V_T	–	0.201	0.203	0.238	0.249
A_{inner}, cm^2	–	66.072	68.514	79.557	91.438
ε	0.88	0.901	0.897	0.881	0.863
$E_{needed,350°C}$ (kJ/s)	0.70	1.29	0.78	0.98	1.06
D_h (10^3 m)	0.29	2.03	1.12	1.78	1.71

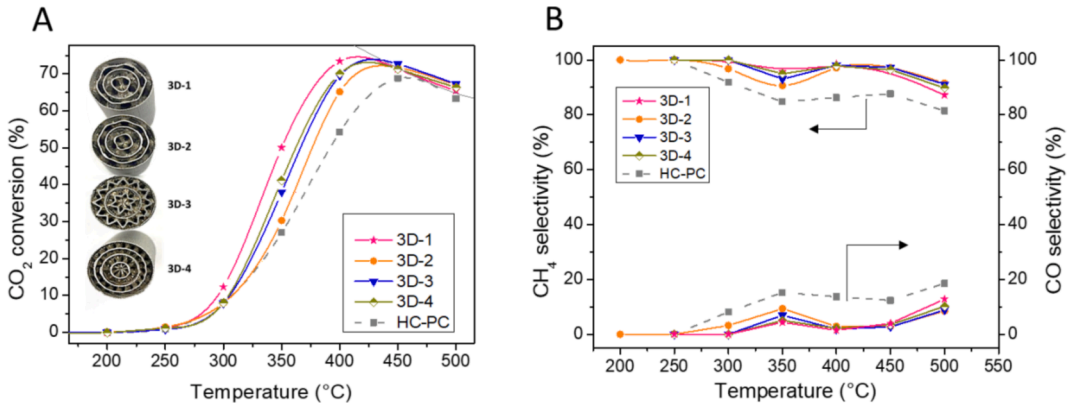

Fig. 7. Catalytic activity of the structured catalyst at 120 L/gh and H_2/CO_2 ratios of 4: A) CO_2 conversion; B) CH_4/CO selectivity.

conversion, the better heat exchange in radial direction.

Along with the geometrical features of the metal substrates, Table 2 also shows the energy associated with the conversion values exhibited by the different structured catalysts at 350 °C. Accordingly, the improved performance displayed by the 3D-1 catalyst implies that the higher void fraction permits, the more efficient usage of the energy supplied by the external heating source. If the void fraction in this FGEs is higher, the velocity of the fluid will be lower than in a FGEs with a lower void fraction, assuming the total flow rate is equal for both cases. At increased velocity the total amount of exchanged heat will be lower in comparison to operating at lower velocity.

Along with the radial heat transfer, the geometry of the FGEs substrate might certainly affect the radial mixing and turbulence established within the catalytic systems. Although putting values to the Re number attained for the different geometries is not an easy task, insights on the mixing regime and turbulence could be extrapolated from the hydraulic diameter values since it should be proportional to the Re number. For the prepared samples, the hydraulic diameter (D_H, Equation (6)) [26] is used as a characteristic dimension, where *h* stands for the length of the metal substrate (30 mm) and $S_{V,SP}$ for the specific surface of the spacer. The impact of the gas mixing and the flow regimes established within the different metal substrates on the catalyst performance is exemplified by the 3D-1 catalyst which exhibited both the greatest conversion rate and radial mixing.

$$D_H \quad \frac{4 \times VolumeofFlowChannel}{Wettedsurface} \quad \frac{4 \times \varepsilon}{\frac{2}{h} + (1 \quad \varepsilon) \times S_{V,SP}} \tag{6}$$

3.1. Prediction model for the best monolith

Fig. 8 shows the CO_2 conversion obtained for the tests previously defined in Table 1. A total of 29 experiments were performed revealing a high influence of the parameters chosen for study, as the variation of the results range from 0 to 62%. The standard deviation of the results is 19.1388.

The experimental results showed in Fig. 8 enable the fit of a mathematical model expressed by Equation (7) for the actual parameters (A_a Actual Temperature; B_a Actual SV; C_a Actual H_2/CO_2 ratio; D_a Actual CO_2 inlet concentration). The resulting model can be used to make predictions of the conversion for given levels of each factor (using the original units). Nonetheless, this model should not be used to determine the relative impact of each factor, as the coefficients are scaled to accommodate each of their units and the intercept is not at the center of the design space.

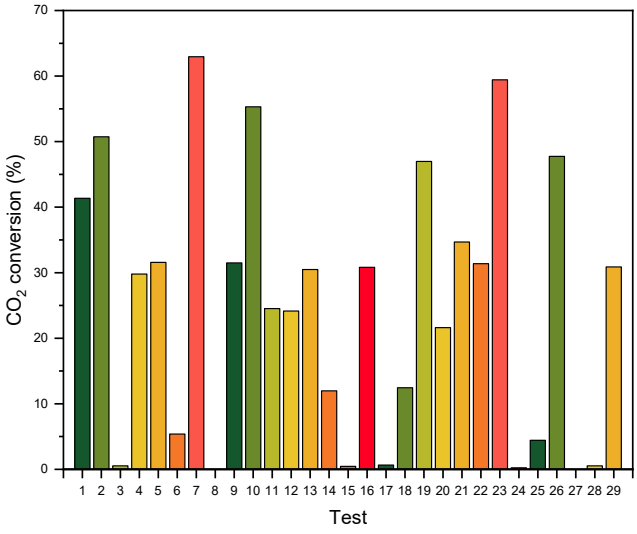

Fig. 8. CO_2 conversion obtained for the experimental matrix carried out for the optimization of the best performing monolith.

To quantify relative impacts, a model in terms of coded factors must be used (Equation (8)), which will make predictions of the conversion for given levels of each factor. By default, the high levels of the factors are coded as + 1 and the low levels of the factors are coded as 1. The coded model is useful for identifying the relative impact of the factors by comparing their coefficients. In this coded equation, the following identification of parameters is needed: A_c Coded Temperature; B_c Coded SV; C_c Coded H_2/CO_2 ratio; D_c Coded CO_2 inlet concentration.

$$CO_2 conversion(\%) \quad 32.38837 + 0.18585 \cdot A_a + \quad 0.13576 \cdot B_a + 14.64781 \cdot C_a + 1.46253 \cdot D_a \quad 0.0000541129 \cdot A_a \cdot B_a + 0.044141 \cdot A_a \cdot C_a$$

$$0.00407987 \cdot A_a \cdot D_a + 0.00139 \cdot B_a \cdot C_a + 0.000592286 \cdot B_a \cdot D_a \quad 0.13947 \cdot C_a \cdot D_a \quad 0.000154797 \cdot A_a^2 + 0.000189826 \cdot B_a^2 \quad 4.08406 \cdot C_a^2 \quad 0.037698 \cdot D_a^2 \tag{7}$$

$$CO_2 conversion(\%) \quad 27.58 + 19.87 \bullet A_c \quad 2.77 \bullet B_c + 3.92 \bullet C_c \quad 6.69 \bullet D_c \quad 0.81 \bullet A_c B_c + 6.62 \bullet A_c C_c \quad 3.06 \bullet A_c D_c + 0.14 \bullet B_c C_c + 0.30 \bullet B_c D_c \quad 3.48 \bullet A_c^2 + 1.90 \bullet B_c^2 \quad 4.08 \bullet C_c^2 \quad 0.94 \bullet D_c^2 \tag{8}$$

Table 3
CO_2 conversion model statistics.

Source	Sum of Squares	df	Mean Square	F-value	p-value
Model	10700.35	14	764.31	13.47	< 0.0001
Temperature factor	6789.87	1	6789.87	119.70	< 0.0001
SV factor	184.79	1	184.79	3.26	0.0878
H_2/CO_2 ratio factor	368.39	1	368.39	6.49	0.0202
CO_2 concentration factor	1197.41	1	1197.41	21.11	0.0002

Table 3 reveals the model statistics obtained for the system and for the individual parameters. A quadratic model with a correlation coefficient (R^2) of 91.29% is proposed. The model's F-value of 13.47 implies that the model is significant. There is only a 0.01% chance that an F-value this large could occur due to noise. The p-value (<0.05) further confirms that the mathematical model obtained is significant. These statistical parameters ensure that the resulting model can serve to predict fairly the CO_2 conversion efficiency within the range studied.

From Equation (7) it can be concluded that the parameter with a higher impact on the CO_2 conversion is the temperature (A in code factors) since its coefficient is the greatest. Therefore, increasing the temperature seems a good strategy to obtain a better CO_2 conversion. Nonetheless, a higher temperature entails higher energy consumption.

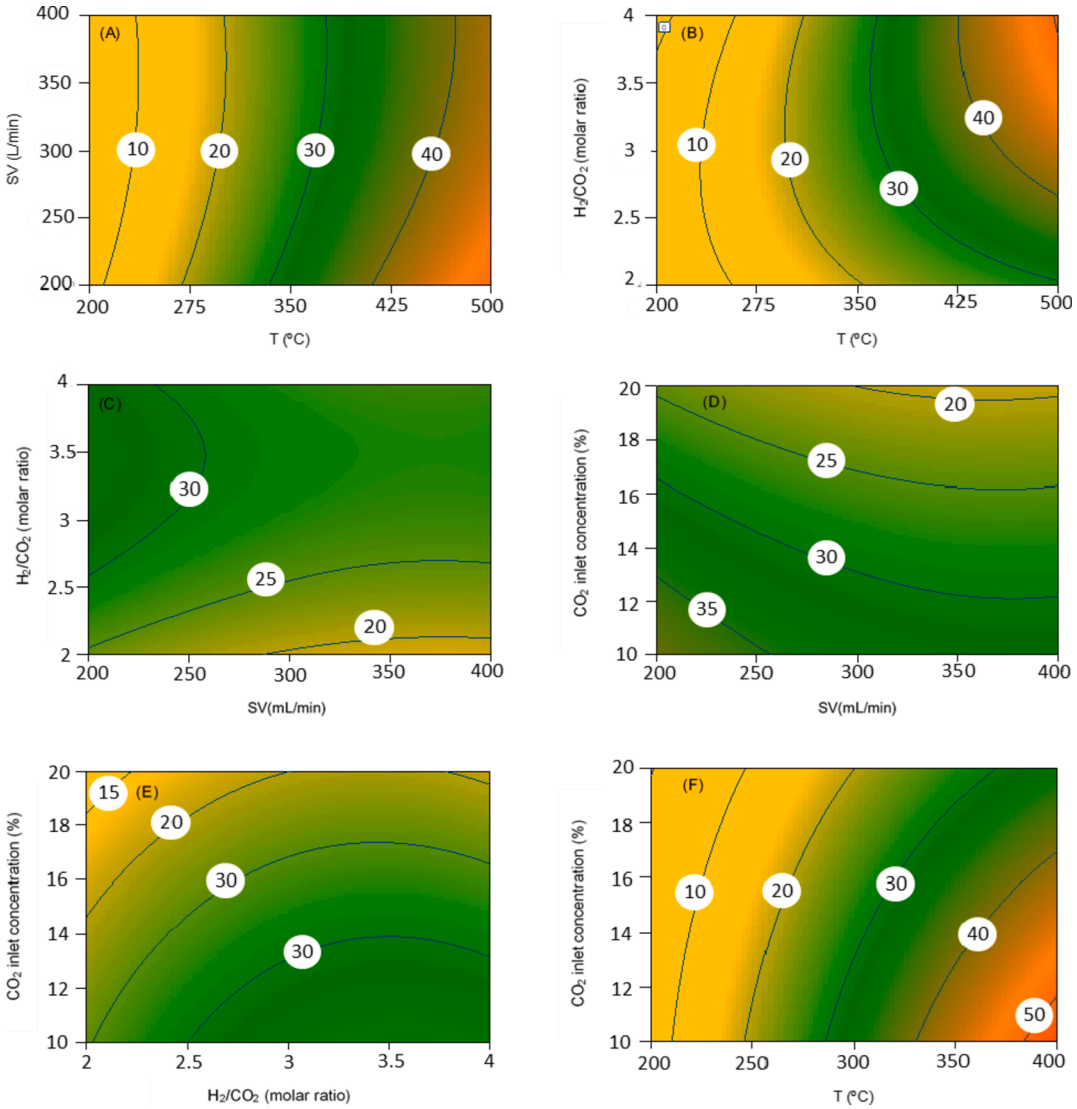

Fig. 9. Two factor model graphs for the CO_2 conversion system for: (A) T-SV, with $H_2/CO_2 = 3$ and CO_2 inlet concentration = 15%; (B) T- H_2/CO_2, with SV = 300 mL/min and CO_2 inlet concentration = 15%; (C) SV- H_2/CO_2, with T = 350 °C and CO_2 inlet concentration = 15%; (D) SV-CO_2 inlet concentration, with T = 350 °C and $H_2/CO_2 = 3$; (E) H_2/CO_2-CO_2 inlet concentration, T = 350 °C and SV = 300 mL/min; and (F) T-CO_2 inlet concentration, with SV = 300 mL/min and $H_2/CO_2 = 3$.

Increasing the H_2/CO_2 ratio can be another potential strategy, but attention must be paid to the extra-cost of the post-separation of CH_4 from the unreacted CO_2 and H_2 and the extra-cost of producing higher flows of hydrogen. Analysing the economic balance between these two parameters is indeed an interesting point to be considered in future works.

Regarding parameters with a negative impact on the performance, SV has the lowest impact, as shown in Equation (7). This is somehow a positive result since the CO_2 conversion would not be highly penalized if higher inlet flows are used, making somehow viable scaling-up to industrial levels, where high flows are more interesting from an operational point of view. Fig. 9 shows the interactions between pairs of parameters, and further reinforces the conclusions drawn about the effect of each parameter on the CO_2 conversion during the methanation reaction. Taking as example Fig. 9A, and for fixed values of the H_2/CO_2 ratio (3) and CO_2 inlet concentration (15%), a joint effect between temperature and SV can be seen. Therefore, increasing the temperature has a positive impact on CO_2 conversion, whereas increasing SV has the opposite effect. This results in CO_2 conversion curves slightly opened to the left side, assuming the total flow rate is equal for both cases. At increased velocity, the total amount of exchanged heat will be lower in comparison to lower velocity. On the contrary, in Fig. 9B, where both parameters have a positive effect on the CO_2 conversion, curves are slightly opened to the right, meaning a positive response of the targeted result with the increase of the variables.

Further confirmation of the results obtained previously can be obtained with the other response surfaces for the pairs T-SV, T- H_2/CO_2, T-CO_2, SV- H_2/CO_2, SV-CO_2 inlet concentration, and H_2/CO_2-CO_2 inlet concentration, and illustrated in Fig. 9. These response surfaces enable the optimization of the CO_2 conversion by tuning the value of the parameters in agreement with the surfaces obtained, which fits a quadratic model. For example, focusing on Fig. 9A, it can be seen that in order to maximize the CO_2 conversion, minimum SV and maximum temperature within the range of study are needed. Equivalent conclusions can be drawn from the rest of the graphs as previously discussed.

The Design-Expert software numerical optimization tool has been used to determine the optimum conversion of CO_2. The software allows one or several variables to be restricted: minimized, maximized, or targeted. The optimization tool searches for the combination of factors that simultaneously satisfy the criteria placed on the response and factors. In this context, the CO_2 conversion has been optimized for three different scenarios:

- Scenario 1, without restrictions. In this case, the operational factors and the optimum CO_2 conversion were: T 497 °C, SV 207 mL/min, H_2/CO_2 3.9 M ratio, inlet CO_2 concentration 10.1 %. With this combination of factors, the CO_2 conversion was 64.2%
- Scenario 2, with two restrictions: temperature as low as possible and H_2/ratio as low as possible. In this case, when T 431 °C, SV 200 mL/min, H_2/CO_2 3 M ratio, and inlet CO_2 concentration 10 % the CO_2 conversion was determined to be 50.1%. Due to the loss of performance, despite the fact that a higher temperature implies a higher energy cost, Scenario 2 is ruled out as the optimal.
- Scenario 3, with one restriction on the H_2/CO_2 ratio (minimize). In this case, the operational factors and the optimum CO_2 conversion were as follows: T 500 °C, SV 200 mL/min, H_2/CO_2 3 M ratio, inlet CO_2 concentration 10 % and CO2 conversion 58.9%.

4. Conclusions

This work investigates the CO_2 methanation performance of 0.5% Ru 15% Ni/$MgAl_2O_4$ structured catalysts by tuning the geometry of 3D-printed metal FGEs structures based on periodically variable pseudo-gyroid structures. The improvement in the activity exhibited by the structured catalysts was enhanced by the radial heat transfer facilitated by optimal FGEs geometries. Thus, the highest porosity attained in the best performing catalyst (3D-1) resulted in enhanced heat usage enabling a significantly improved catalytic behavior with ca. 25% higher conversion values within the intermediate temperature range. The improved radial heat transfer of the 3D-1 system permitted attaining conversion values of ca. 75% CO_2 at 400 °C and 120 L/(gh). Furthermore, the mathematical model obtained through Experimental Design enabled the prediction of the behavior of the 3D-1 structured catalyst and the determination of the optimal operating conditions under different scenarios of interest. Thus, minimizing the temperature and H_2/CO_2 ratio, the model projected that the best CO_2 methanation conditions for the 3D-1 catalyst involves operating at 431 °C, 200 mL/min, H_2/CO_2 3 M ratio, and inlet CO_2 concentration 10 %.The benefits provided by FGEs will be further explored and the impact of the substrate material, the geometry and number of modules should be analysed.

5. 3D printing for CO_2 methanacion catalysts: A short outlook

The efforts and number of research aiming at the development and manufacture of CO_2 methanation catalysts by 3D-printing technologies will expectedly increase. Additive manufacturing arises as a promising tool towards the progress of technologies for SNG production since it enables better control of catalyst structures and catalyst distribution. The current status of 3D-printing technologies, the types of additive manufacturing and the general perspective of additive manufacturing applied to catalysis has been recently highlighted by a few excellent works [19,21,27–30]. For the CO_2 methanation reaction, investigations dealing with widening the palette of printable materials with controlled structural features is projected as an important field. In this context, advances on 3D-printing technologies that permit directly printing MOFs, COFs and even graphene might be of interest. Another important research line to consider will verge around the substrate functionalization with a catalysts anchored to the surface (the so-called 4D-printing), and will certainly grab the attention [31]. This approach might prove a breackthrough for a number of catalytic processes and it could deliver layered multi-functional catalysts, with highly-dispersed and well-inmobilized active phases. Furthermore, the majority of CO_2 methanation structured catalysts are based on periodic and regular geometries. Assisted by Computer Fluid Dynamic (CFD), significant efforts will be devoted to shape engineering the next generation of catalytic systems with tunned microfluidic and optimal performances. For instance, solutions mimicking nature-inspired geometries for modulating the rheological properties of the catalytic systems, thereby cve been recently proposed.

Declaration of Competing Interest

The authors declare that they have no known competing financial interests or personal relationships that could have appeared to influence the work reported in this paper.

Acknowledgments and Funding

This work was supported by University of Seville through V PPIT-US.

Appendix A. Supplementary data

Supplementary data to this article can be found online at https://doi.org/10.1016/j.enconman.2022.115464.

References

[1] Li S, Gong J. Strategies for improving the performance and stability of Ni-based catalysts for reforming reactions. Chem Soc Rev 2014;43:7245–56. https://doi.org/10.1039/c4cs00223g.
[2] Frontera P, Macario A, Monforte G, Bonura G, Ferraro M, Dispenza G, et al. The role of Gadolinia Doped Ceria support on the promotion of CO2 methanation over

Ni and Ni–Fe catalysts. Int J Hydrogen Energy 2017;42:26828–42. https://doi.org/10.1016/j.ijhydene.2017.09.025.
[3] Le TA, Kim MS, Lee SH, Kim TW, Park ED. CO and CO2 methanation over supported Ni catalysts. Catal Today 2017;293–294:89–96. https://doi.org/10.1016/j.cattod.2016.12.036.
[4] Frontera P, Macario A, Ferraro M, Antonucci PL. Supported catalysts for CO2 methanation: A review. Catalysts 2017;7:1–28. https://doi.org/10.3390/catal7020059.
[5] Baena-Moreno FM, Zhang Z, Zhang XP, Reina TR. Profitability analysis of a novel configuration to synergize biogas upgrading and Power-to-Gas. Energy Convers Manag 2020;224:113369.
[6] Balzarotti R, Ambrosetti M, Arnesano M, Anglani A, Groppi G, Tronconi E. Periodic open cellular structures (POCS) as enhanced catalyst supports: Optimization of the coating procedure and analysis of mass transport. Appl Catal B Environ 2021;283:119651. https://doi.org/10.1016/j.apcatb.2020.119651.
[7] Schollenberger D, Bajohr S, Gruber M, Reimert R, Kolb T. Scale-up of innovative honeycomb reactors for power-to-gas applications – the project store&go. Chem-Ing-Tech 2018;90:696–702. https://doi.org/10.1002/cite.201700139.
[8] González-Castano M, Ivanova S, Laguna OH, Martínez T. LM, Centeno MA, Odriozola JA. Structuring Pt/CeO2/Al2O3 WGS catalyst: Introduction of buffer layer. Appl Catal B Environ 2017;200:420–7.
[9] González-Castano M, Reina TR, Ivanova S, Martínez Tejada LM, Centeno MA, Odriozola JA. O2-assisted Water Gas Shift reaction over structured Au and Pt catalysts. Appl Catal B Environ 2016;185:337–43. https://doi.org/10.1016/j.apcatb.2015.12.032.
[10] Tronconi E, Groppi G, Visconti CG. Structured catalysts for non-adiabatic applications. Curr Opin Chem Eng 2014;5:55–67. https://doi.org/10.1016/j.coche.2014.04.003.
[11] Bracconi M, Ambrosetti M, Maestri M, Groppi G, Tronconi E. A fundamental investigation of gas/solid mass transfer in open-cell foams using a combined experimental and CFD approach. Chem Eng J 2018;352:558–71. https://doi.org/10.1016/j.cej.2018.07.023.
[12] Echave FJ, Sanz O, Velasco I, Odriozola JA, Montes M. Effect of the alloy on micro-structured reactors for methanol steam reforming. Catal Today 2013;213:145–54. https://doi.org/10.1016/j.cattod.2013.02.027.
[13] Almeida LC, Sanz O, Merino D, Arzamendi G, Gandía LM, Montes M. Kinetic analysis and microstructured reactors modeling for the Fischer-Tropsch synthesis over a Co-Re/Al2O3 catalyst. Catal Today 2013;215:103–11. https://doi.org/10.1016/j.cattod.2013.04.021.
[14] González-Castano M, Dorneanu B, Arellano-García H. The reverse water gas shift reaction: a process systems engineering perspective. React Chem Eng 2021;6(6):954–76.
[15] Baena-Moreno FM, González-Castano M, Navarro de Miguel JC, Miah KUM, Ossenbrink R, Odriozola JA, et al. Stepping toward Efficient Microreactors for CO 2 Methanation: 3D-Printed Gyroid Geometry. ACS Sustain Chem Eng 2021;9(24):8198–206.
[16] Navarro JC, Centeno MA, Laguna OH, Odriozola JA. Ru–Ni/MgAl2O4 structured catalyst for CO2 methanation. Renew Energy 2020;161:120–32. https://doi.org/10.1016/j.renene.2020.07.055.
[17] Ricca A, Truda L, Palma V. Study of the role of chemical support and structured carrier on the CO2 methanation reaction. Chem Eng J 2019;377:120461.
[18] García-Moncada N, Navarro JC, Odriozola JA, Lefferts L, Faria JA. Enhanced catalytic activity and stability of nanoshaped Ni/CeO2 for CO2 methanation in micro-monoliths. Catal Today 2022;383:205–15.
[19] Hurt C, Brandt M, Priya SS, Bhatelia T, Patel J, Selvakannan PR, et al. Combining additive manufacturing and catalysis: A review, Catal. Sci Technol 2017;7:3421–39. https://doi.org/10.1039/c7cy00615b.
[20] Danaci S, Protasova L, Lefevere J, Bedel L, Guilet R, Marty P. Efficient CO2 methanation over Ni/Al2O3 coated structured catalysts. Catal Today 2016;273:234–43. https://doi.org/10.1016/j.cattod.2016.04.019.
[21] Parra-Cabrera C, Achille C, Kuhn S, Ameloot R. 3D printing in chemical engineering and catalytic technology: Structured catalysts, mixers and reactors. Chem Soc Rev 2018;47:209–30. https://doi.org/10.1039/c7cs00631d.
[22] Hansjosten E, Wenka A, Hensel A, Benzinger W, Klumpp M, Dittmeyer R. Custom-designed 3D-printed metallic fluid guiding elements for enhanced heat transfer at low pressure drop. Chem Eng Process - Process Intensif 2018;130:119–26. https://doi.org/10.1016/j.cep.2018.05.022.
[23] Álvarez MA, Bobadilla LF, Garcilaso V, Centeno MA, Odriozola JA. CO2 reforming of methane over Ni-Ru supported catalysts: On the nature of active sites by operando DRIFTS study. J CO2 Util 2018;24:509–15. https://doi.org/10.1016/j.jcou.2018.01.027.
[24] A. Hensel, A. Wenka, E. Hansjosten, W. Benzinger, Flow guide in a channel, DE102015113432A1, 2016.
[25] Italiano C, Llorca J, Pino L, Ferraro M, Antonucci V, Vita A. CO and CO2 methanation over Ni catalysts supported on CeO2, Al2O3 and Y2O3 oxides. Appl Catal B Environ 2020;264:118494. https://doi.org/10.1016/j.apcatb.2019.118494.
[26] Schock G, Miquel A. Mass transfer and pressure loss in spiral wound modules. Deaslination 1987;64:339–52.
[27] Chaparro-Garnica CY, Jordá-Faus P, Bailón-García E, Ocampo-Pérez R, Aguilar-Madera CG, Davó-Quinonero A, et al. Customizable heterogeneous catalysts: nonchanneled advanced monolithic supports manufactured by 3D-printing for improved active phase coating performance. ACS Appl Mater Interfaces 2020;12:54573–84. https://doi.org/10.1021/acsami.0c14703.
[28] Zhou X, Liu C-J. Three-dimensional printing for catalytic applications: current status and perspectives. Adv Funct Mater 2017;27(30):1701134.
[29] M. Zhang, M. Ng, X. Yi, B.Z. Hong, L. Che, B. Chen, CFD simulation of methanation reaction over 3D-printed monolithic catalysts : A comparative study, (n.d.).
[30] Lawson S, Li X, Thakkar H, Rownaghi AA, Rezaei F. Recent advances in 3D printing of structured materials for adsorption and catalysis applications. Chem Rev 2021;121:6246–91. https://doi.org/10.1021/acs.chemrev.1c00060.
[31] Kuang X, Chen K, Dunn CK, Wu J, Li VCF, Qi HJ. 3D printing of highly stretchable, shape-memory, and self-healing elastomer toward novel 4D printing. ACS Appl Mater Interfaces 2018;10(8):7381–8.